SUPPLEMENTAL INFORMATION

Assembly of BRG1–G9a/GLP–DNMT3 repressive chromatin complex on *Myh6* in pathologically stressed hearts

Pei Han[+], Wei Li[+], Jin Yang, Ching Shang, Chiou-Hong Lin, Wei Cheng, Calvin T. Hang, Hsiu-Ling Cheng, Chen-Hao Chen, Johnson Wong, Yiqin Xiong, Mingming Zhao, Stavros G. Drakos, Andrea Ghetti, Dean Y. Li, Daniel Bernstein, Huei-sheng Vincent Chen, Thomas Quertermous, Ching-Pin Chang[*]

SUPPLEMENTAL TEXT

H3K9 methylation

Lysine at position 9 along the histone 3 tail can be modified to a mono- (H3K9me1), di- (H3K9me2) or tri-methylated state (H3K9me3). Although both di-, and tri-methylation of Histone H3 lysine 9 (H3K9) are essential repressive chromatin modification, H3K9me2 has different regulatory roles from H3K9me3. H3K9me2 is of particular interest because it is critical for silencing euchromatin within gene-rich areas across the genome (Kubicek et al., 2007; Sharma et al., 2012). In contrast, H3K9me3 marks heterochromatin and is mainly localized to the gene-poor regions of repetitive DNA. Furthermore, H3K9me2 is associated directly with gene repression (Sharma et al., 2012; Wen et al., 2009). Given that *Myh6* and *Myh7* are actively regulated genes in the heart, H3K9me2 appears more likely to be the critical mark for *Myh* genes, and our data support that H3K9me2 and G9a/Glp play essential roles in cardiac gene repression, hypertrophy, and dysfunction.

H3K9 methyltransferase

In mammals, H3K9 methylation requires the histone lysine methyltransferase (HKMT) family, consisting of Ehmt1/Glp, Ehmt2/G9a, Suv39h1, Suv39h2, Setdb1 and Setdb2, as well as the non-Suv39 enzymes Prdm2 and Ash1L (Wu et al., 2010). Among all known HKMTs, G9a and GLP—which form a heterodimeric complex—are the major HKMTs for H3K9 methylation on euchromatin (Shinkai and Tachibana, 2011). Setdb1 and 2 are also HKMTs which catalyze H3K9 methylation on euchromatin. In contrast, Suv39h1 and 2 are primary HKMTs that target the pericentric heterochromatin. Prdm2 functions as a tumor suppressor (Kim et al., 2003). Ash1L, on the other hand, is not specific for H3K9; it

also methylates H3K4, H4K20, and H3K36 and therefore could have both repressive and active functions for gene expression (An et al., 2011; Gregory et al., 2007; Wu et al., 2010).

DNMT

DNA cytosine-5 methyltransferases (DNMTs) catalyze the transfer of a methyl group to the CpG sites of DNA. In mammals, three active DNMTs have been identified—Dnmt1, Dnmt3a, and Dnmt3b (Bestor, 2000; Jaenisch and Bird, 2003; Li, 2002). Dnmt1 methylates the hemimethylated CpG di-nucleotides in the mammalian genome during DNA replication to maintain DNA methylation during cell proliferation. In contrast, Dnmt3a and Dnmt3b are the methyltransferases that catalyze *de novo* DNA methylation (Li et al., 1992; Okano et al., 1999). Consistent with cardiomyocytes being primarily post-mitotic, only the *de novo* Dnmt3a and 3b—but not the maintenance Dnmt1—methyltransferases are induced in the cardiomyocytes after pressure overload (Figures 2G, and S2C–S2F). Dnmt3a and Dnmt3b have distinct enzymatic properties (Suetake et al., 2003; Takeshima et al., 2006), and these two isoforms target both overlapping and specific regions *in vivo* (Chen et al., 2003; Kaneda et al., 2004; Okano et al., 1999; Xu et al., 1999).

Necessity of both H3K9 and CpG methylation for Myh6 silencing

BIX inhibits G9a enzymatic activity to disrupt H3K9me2 formation. By inhibiting H3K9me2 but without affecting CpG methylation, BIX was capable of de-repressing *Myh6* and reducing hypertrophy (Figures S3A–S3J), indicating that H3K9me2 is

functionally essential for silencing *Myh6*. On the other hand, AZA or Dnmt3 disruption had no effects on H3K9me2; yet both AZA and Dnmt3 disruption de-repressed *Myh6* and reduced hypertrophy, suggesting that CpG methylation, like H3K9me2, is essential for *Myh6* silencing (Figures S3A–S3J, and S5A–S5J). Knocking down either H3K9me2 or CpG methylation caused de-repression of *Myh6* and reduction of hypertrophy. Therefore, both H3K9me2 and CpG methylation are required, and these modifications cooperate to silence *Myh6* in stressed hearts.

SUPPLEMENTAL EXPERIMENTAL PROCEDURES

Morphometric analysis of cardiomyocytes

Paraffin sections of the heart were immunostained with a fluorescein isothiocyanate-conjugated Wheat Germ Agglutinin (WGA) antibody (F49, Biomeda, Foster City, CA) that highlighted the cell membrane of cardiomyocytes. Cellular areas outlined by WGA were determined by the number of pixels enclosed using the NIS element software (Nikon). Approximately 250 cardiomyocytes of the papillary muscle at the mid left ventricular cavity were measured to determine the size distribution. P-values were calculated by the Student-t test. Error bars indicate standard error of mean.

Reverse transcription–quantitative PCR analysis (RT–qPCR)

RT–qPCR analyses were performed as described previously(Hang et al., 2010; Stankunas et al., 2008). The following primer sequences (listed below) were used. RT–qPCR reactions were performed using SYBR green master mix (BioRad, Hercules, CA) with an Eppendorf realplex, and the primer sets were tested to be quantitative. Threshold cycles and melting curve measurements were performed with software. P-values were calculated by the Student-t test. Error bars indicate standard error of mean.

PCR primers for* RT–qPCR *of mRNA:

Mouse *G9a*-F (CAGCCGAGCACAAGCACATC),
Mouse *G9a*-R (CTCCACGAGACAGGAACAACA),
Mouse *Glp*-F (GTCTGGTCACGCTCCTGTAT),
Mouse *Glp*-R (AAGCAAACCCACATTTCATC),
Mouse *Dnmt3a*-F (CACACCTGAGCTGTACTGCAGAG),
Mouse *Dnmt3a*-R (CTCTTCCACAGCATTCATTACTGC),
Mouse *Dnmt3b*-F (ACCAAATCCAGGGCCTTCTTT),
Mouse *Dnmt3b*-R (GATAATGCACTCCTCATACCCGC),
Mouse *Suv39h1*-F (CTGTGCCGACTAGCCAAGC),
Mouse *Suv39h1*-R (ATACCCACGCCACTTAACCAG),

Mouse *Suv39h2*-F (GCTGTGGTTGGGGTGTAAAA),
Mouse *Suv39h2*-R (GCTGCATCCACTGTGAACTC),
Mouse *Setdb1*-F (GATTCTGGGCAAGAAGAGGA),
Mouse *Setdb1-R* (GTACTTGGCCACCACTCGAC),
Mouse *Setdb2*-F (TCAGTCGCGTTTCCCCCACC),
Mouse *Setdb2*-R (CAAGGCCAGGTTGAAAGCCGGA),
Mouse *Hdac1*-F (GCGAGACGGCATTGACGACGA),
Mouse *Hdac1*-R (GTCCAGGGCCACCGCTGTTT),
Mouse *Hdac2*-F (GCCAGGGTCATCCCATGAAGCC),
Mouse *Hdac2*-R (CCCCAGCAACTGAACCACCCG),
Mouse *Hdac3*-F (GACTGACGAGGCCGACGCTG),
Mouse *Hdac3*-R (ACACCCTGGGGGTACCCAGTT),
Mouse *Parp1*-F (CCCCACCTGAAGCGCCTGTG),
Mouse *Parp1*-R (CCAGGGTGATGCTGGCCGA),
Mouse *Myh6*-F (GCAGGCCCTGGCTCTTCAGC),
Mouse *Myh6*-R (GCCTGCCTCCTCCAGCCTCT),
Mouse *Myh7*-F (GCCCTTTGACCTCAAGAAAG),
Mouse *Myh7*-R (CTTCACAGTCACCGTCTTGC),
Mouse *TFIIb*-F (CTCTGTGGCGGCAGCAGCTATTT),
Mouse *TFIIb*-R (CGAGGGTAGATCAGTCTGTAGGA),
Human *G9a*-F (GCGAAAAGACAGCCCATGGGTG),
Human *G9a*-R (GCCTGAGGAGCCCACACCATTC),
Human *GLP*-F (GGCGGGCGCTAATATTGACACCT),
Human *GLP*-R (TTGGCAGCCAGGTGCAAACACG),
Human *DNMT3a*-F (TATTGATGAGCGCACAAGAGAGC),
Human *DNMT3a*-R (GGGTGTTCCAGGGTAACATTGAG),
Human *DNMT3b*-F (GACTTGGTGATTGGCGGAA),
Human *DNMT3b*-R (GGCCCTGTGAGCAGCAGA),
Human *HDAC1*-F (GGCGAGCAAGATGGCGCAGA),
Human *HDAC1*-R (TCTGGACGGATGGAGCGCAAGA),
Human *HDAC2*-F (CGGGGAGCCCATGGCGTACA),
Human *HDAC2*-R (TTCGGCAGTGGCTTTATGGGGC),
Human *HDAC3*-F (ACCGGGTCATGACGGTGTCCT),
Human *HDAC3*-R (ACGCATTCCCCATGCCCTCG),
Human *PARP1*-F (AGGTCCAGCAGGCGGTGTCT),
Human *PARP1*-R (TTCCGCCTTGGCCTGCACAC),
Human *MYH6*-F (GGCCACTCTCTTCTCCTCCTACGC),
Human *MYH6*-R (GGTGGAGAGCCGACACCGTC),
Human *MYH7*-F (CTGCGGCTGCAGGACCTGG),
Human *MYH7*-R (CTCATTCAAGCCCTTCGTGCCA),
Human *ANF*-F (GCGGAGATCCAGCTGCTTCGG),
Human *ANF*-R (GGGAGAGGCGAGGAAGTCACCA),
Human *BNP*-F (TTCCTGGGAGGTCGTTCCCAC),
Human *BNP*-R (CATCTTCCTCCCAAAGCAGCC),
Human *TFIIb*-F (ACCACCCCAATGGATGCAGACAG),
Human *TFIIb*-R (ACGGGCTAAGCGTCTGGCAC).

Sequential chromatin immunoprecipitation (reChIP)

Ventricles harvested from adult mice were performed for reChIP experiment 7 days after sham or TAC operations. Anti-BRG1 H10 antibody (Cat# sc-374197X, Santa Cruz

Biotechnology) was immobilized with protein G sepharose beads (P3296, Sigma-Aldrich) by disuccinimidyl suberate (DSS). DSS were inactivated by 0.1 M ethanolamine. Non-crosslinked antibodies were removed by 0.1M glycine (pH 2.8), and the supernatant was neutralized by 1M Tris-base (pH 8.8), followed by 3 times wash of sodium borate washing solution (50 mM, pH 8.2). Immobilized antibody was incubated with sonicated chromatin from hearts overnight at 4 °C. The Brg1-immunoprecipitated chromatin was then purified according to the manufacturer's protocol (17-295, Millipore). Immunoprecipitated chromatin was eluted by 10 mM DTT (30 min, 30 °C). The eluates were then diluted with ChIP dilution buffer (17-295, Millipore). Normal control IgG, anti-G9a or anti-Dnmt3a antibody was used for the secondary ChIP. The immunoprecipitated chromatin was further purified, and ChIP-qPCR analysis of *Myh6* and *Myh7* promoters was then performed.

Western blot analysis

The blots were reacted with antibodies of anti-G9a (Cat# PP-A8620A-00, R&D Systems), anti-GLP (Cat# PP-B0422-00, R&D Systems), anti-DNMT3a antibody (H-295, Cat# sc20703, Santa Cruz Biotechnology), and anti-DNMT3b (Cat# ab16049, Abcam), followed by HRP-conjugated secondary antibodies (Jackson ImmunoResearch Laboratories, West Grove, PA). Chemiluminescence was detected with ECL Western blot detection kits (GE).

Co-immunoprecipitation

Adult mouse heart ventricles were minced and homogenized by cell extraction buffer (25 mM Hepes pH 7.5, 25 mM KCl, 0.1% NP-40, 1 mM DTT, protease inhibitor) to enrich

nuclei. The nuclei were then washed and lysed using nuclear lysis buffer (50 mM Tris-HCl pH 8.0, 150 mM NaCl, 0.1% NP-40, 1 mM DTT, protease inhibitor). The lysates were pre-cleared with PureProteome Protein G Magnetic Beads (Cat# LSKMAGG02, Millipore). Immuunoprecipitation with antibody and following western blotting were performed as described above and previously (Hang et al., 2010). 2 μg primary antibodies of anti-BRG1 (G-7, Cat# sc17796, Santa Cruz Biotechnology), anti-G9a (Cat# PP-A8620A-00, R&D Systems), anti-DNMT3a antibody (H-295, Cat# sc20703, Santa Cruz Biotechnology) or normal control IgG, were used.

Drug treatment

For BIX studies, mice were implanted with subcutaneous micro-osmotic pumps (Alzet Model 1002, DURECT, Cupertino, CA) to infuse BIX01294 (BIX, 25 mg/ml, Cat# 3364, Tocris Bioscience). Micro-pumps were activated prior to implantation to initiate continuous delivery (0.25 μl per hour) of vehicle (PBS) or BIX. Sham or TAC procedures were performed 12 hours post implantation of pumps. After 14 days of sham or TAC operation, mice were evaluated by echocardiography for heart function and harvested for cardiac hypertrophy and fibrosis studies.

For AZA studies, mice were injected intraperitoneally and daily with vehicle (PBS) or 5-Azacytidine (AZA, 2.5 mg/kg/day) (Cat# A2385, Sigma). Sham or TAC procedures were performed 12 hours after the first injection. After 14 days of the sham or TAC operation, mice were evaluated by echocardiography for heart function and harvested for cardiac hypertrophy and fibrosis studies.

For studies of heart tissues harvested 2 days after the sham or TAC operation, mice were injected intraperitoneally and daily with vehicle (PBS), BIX (1 mg/kg/day), or AZA (2.5 mg/kg/day). Sham or TAC operation was performed 12 hours after the first injection. Two days after the operation, hearts were harvested for bisulfate genomic sequencing, RT–qPCR, immunostaining, or ChIP analysis.

Human heart tissue analysis

The human tissues were processed for RT–qPCR, ChIP–qPCR, and bisulfite genomic sequencing analysis as described in above sections. Only de-identified human tissues were used in this study. The use of human tissues is in compliance with the regulation of Sanford/Burnham Medical Research Institute, Intermountain Medical Center, and Stanford University. IRB protocol was approved by Stanford University.

SUPPLEMENTAL REFERENCES

An, S., Yeo, K.J., Jeon, Y.H., and Song, J.J. (2011). Crystal structure of the human histone methyltransferase ASH1L catalytic domain and its implications for the regulatory mechanism. The Journal of biological chemistry *286*, 8369-8374.

Bestor, T.H. (2000). The DNA methyltransferases of mammals. Human molecular genetics *9*, 2395-2402.

Chen, T., Ueda, Y., Dodge, J.E., Wang, Z., and Li, E. (2003). Establishment and maintenance of genomic methylation patterns in mouse embryonic stem cells by Dnmt3a and Dnmt3b. Mol Cell Biol *23*, 5594-5605.

Gregory, G.D., Vakoc, C.R., Rozovskaia, T., Zheng, X., Patel, S., Nakamura, T., Canaani, E., and Blobel, G.A. (2007). Mammalian ASH1L is a histone methyltransferase that occupies the transcribed region of active genes. Molecular and Cellular Biology *27*, 8466-8479.

Hang, C.T., Yang, J., Han, P., Cheng, H.L., Shang, C., Ashley, E., Zhou, B., and Chang, C.P. (2010). Chromatin regulation by Brg1 underlies heart muscle development and disease. Nature *466*, 62-67.

Jaenisch, R., and Bird, A. (2003). Epigenetic regulation of gene expression: how the genome integrates intrinsic and environmental signals. Nature genetics *33 Suppl*, 245-254.

Kaneda, M., Okano, M., Hata, K., Sado, T., Tsujimoto, N., Li, E., and Sasaki, H. (2004). Essential role for de novo DNA methyltransferase Dnmt3a in paternal and maternal imprinting. Nature *429*, 900-903.

Kim, K.C., Geng, L., and Huang, S. (2003). Inactivation of a histone methyltransferase by mutations in human cancers. Cancer research *63*, 7619-7623.

Kubicek, S., O'Sullivan, R.J., August, E.M., Hickey, E.R., Zhang, Q., Teodoro, Miguel L., Rea, S., Mechtler, K., Kowalski, J.A., Homon, C.A.*, et al.* (2007). Reversal of H3K9me2 by a Small-Molecule Inhibitor for the G9a Histone Methyltransferase. Molecular Cell *25*, 473-481.

Li, E. (2002). Chromatin modification and epigenetic reprogramming in mammalian development. Nature reviews Genetics *3*, 662-673.

Li, E., Bestor, T.H., and Jaenisch, R. (1992). Targeted mutation of the DNA methyltransferase gene results in embryonic lethality. Cell *69*, 915-926.

Okano, M., Bell, D.W., Haber, D.A., and Li, E. (1999). DNA methyltransferases Dnmt3a and Dnmt3b are essential for de novo methylation and mammalian development. Cell *99*, 247-257.

Sharma, R.P., Gavin, D.P., and Chase, K.A. (2012). Heterochromatin as an incubator for pathology and treatment non-response: implication for neuropsychiatric illness. Pharmacogenomics J.

Shinkai, Y., and Tachibana, M. (2011). H3K9 methyltransferase G9a and the related molecule GLP. Genes & development *25*, 781-788.

Stankunas, K., Hang, C.T., Tsun, Z.Y., Chen, H., Lee, N.V., Wu, J.I., Shang, C., Bayle, J.H., Shou, W., Iruela-Arispe, M.L.*, et al.* (2008). Endocardial Brg1 represses ADAMTS1 to maintain the microenvironment for myocardial morphogenesis. Developmental cell *14*, 298-311.

Suetake, I., Miyazaki, J., Murakami, C., Takeshima, H., and Tajima, S. (2003). Distinct enzymatic properties of recombinant mouse DNA methyltransferases Dnmt3a and Dnmt3b. J Biochem *133*, 737-744.
Takeshima, H., Suetake, I., Shimahara, H., Ura, K., Tate, S., and Tajima, S. (2006). Distinct DNA methylation activity of Dnmt3a and Dnmt3b towards naked and nucleosomal DNA. J Biochem *139*, 503-515.
Wen, B., Wu, H., Shinkai, Y., Irizarry, R.A., and Feinberg, A.P. (2009). Large histone H3 lysine 9 dimethylated chromatin blocks distinguish differentiated from embryonic stem cells. Nat Genet *41*, 246-250.
Wu, H., Min, J., Lunin, V.V., Antoshenko, T., Dombrovski, L., Zeng, H., Allali-Hassani, A., Campagna-Slater, V., Vedadi, M., Arrowsmith, C.H.*, et al.* (2010). Structural biology of human H3K9 methyltransferases. PloS one *5*, e8570.
Xu, G.L., Bestor, T.H., Bourc'his, D., Hsieh, C.L., Tommerup, N., Bugge, M., Hulten, M., Qu, X., Russo, J.J., and Viegas-Pequignot, E. (1999). Chromosome instability and immunodeficiency syndrome caused by mutations in a DNA methyltransferase gene. Nature *402*, 187-191.

SUPPLEMENTAL FIGURES AND LEGENDS

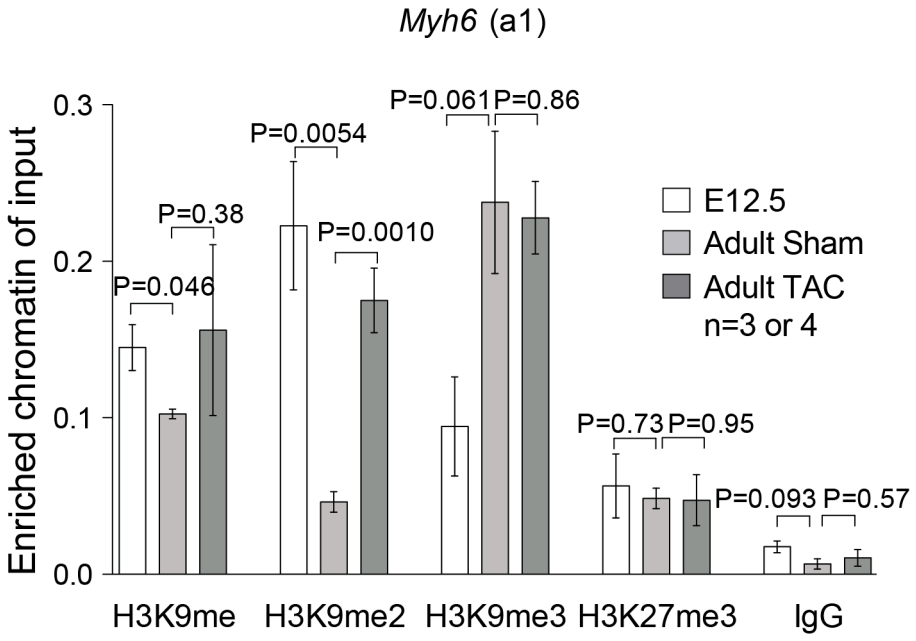

Supplemental Figure S1. Screening of repressive histone methylation on immediate promoter of *Myh6*. Quantitation of H3K9m, H3K9me2, H3K9me3, H3K27me3, and normal IgG ChIP of the proximal promoter of *Myh6* in fetal hearts (E12.5), sham-operated adult hearts, and TAC-operated adult hearts. Data are presented as enrichment relative to input chromatin. P-value: Student's t-test. Error bar: SEM, standard error of the mean.

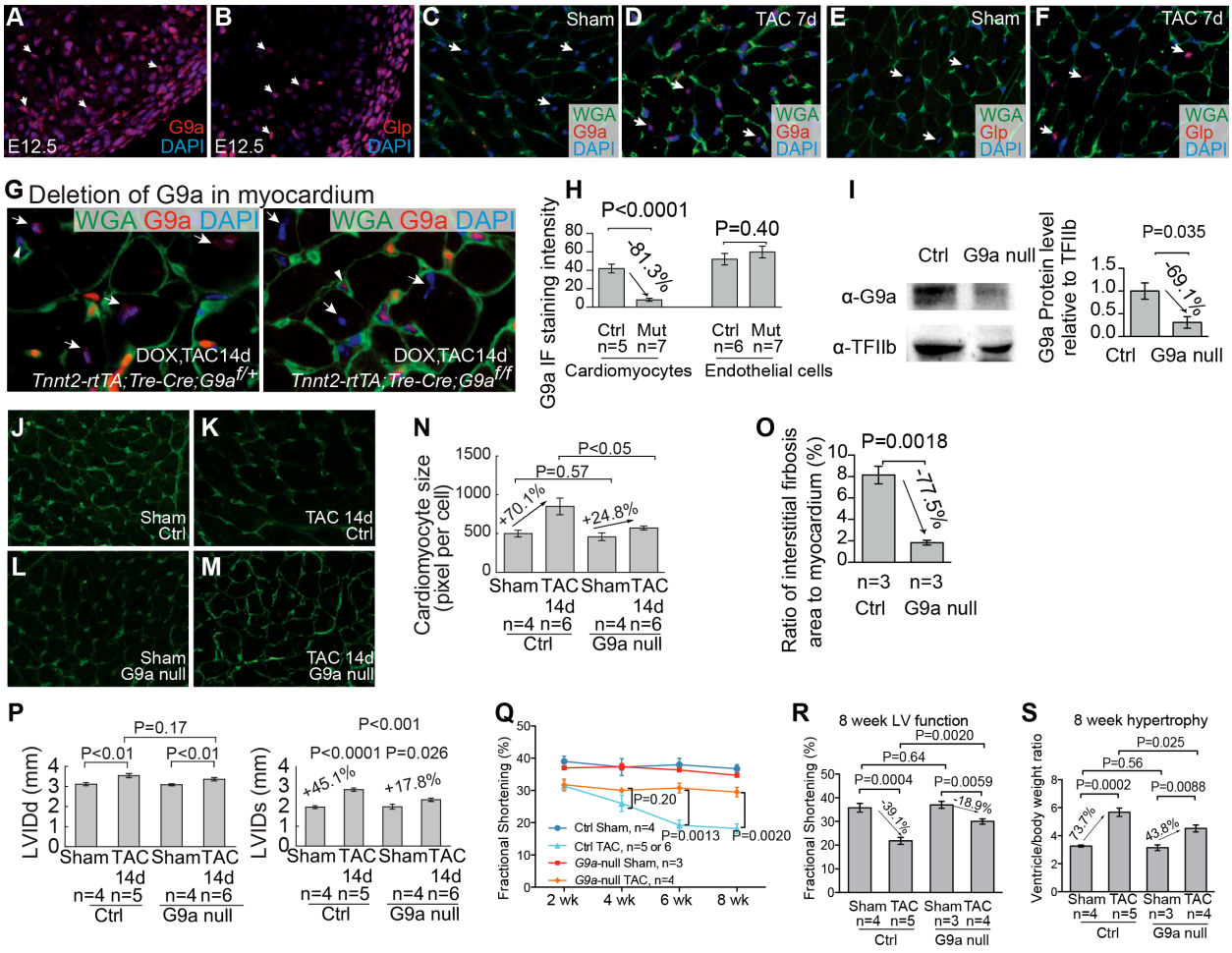

Supplemental Figure S2. Phenotype of the G9a conditional KO mice. (A and B) Immunostaining of G9a and Glp in E12.5 left ventricle. Red: G9a or Glp immunostaining. Blue: DAPI nuclear staining. Arrows point to nuclei of cardiomyocytes. (C–F) Immunostaining of G9a (C and D) and Glp. (E and F) in adult hearts 7 days after sham or TAC procedure. Green: wheat germ agglutinin staining (WGA) outlining cell borders. Red: G9a or Glp immunostaining. Blue: DAPI nuclear staining. Arrows point to nuclei of cardiomyocytes. (G) Immunostaining of G9a in doxycycline (DOX)-treated littermate control (*Tnnt2-rtTA;Tre-Cre;G9a*$^{f/+}$) and G9a-null (*Tnnt2-rtTA;Tre-Cre;G9a*$^{f/f}$) hearts 14 days after TAC. The staining shows the absence of G9a proteins in cardiomyocytes (arrows) but not endothelial cells (arrowheads) in the heart of DOX-treated *Tnnt2-rtTA;Tre-Cre;G9a*$^{f/f}$ mice. Green: wheat germ agglutinin staining (WGA) outlining cell borders. Red: G9a immunostaining. Blue: DAPI nuclear staining. (H) Quantification of G9a immunofluorescence staining of control and G9a-null mice lacking myocardial *G9a* 14 days after TAC operation. Ctrl: control mice. G9a-null: *Tnnt2-rtTA;Tre-Cre;G9a*$^{f/f}$ mice. (I) Western blot and quantification of G9a in the ventricles of control and G9a-null mice lacking myocardial *G9a* 14 days after TAC operation. Ctrl: control mice. G9a-null: *Tnnt2-rtTA;Tre-Cre;G9a*$^{f/f}$ mice. (J–N) Wheat germ agglutinin (WGA) immunostaining of control mice (J and L), G9a-null mice lacking myocardial *G9a* (K and M), and the cardiomyocyte size quantification (N) 14 days after sham or TAC operation. Ctrl: control mice. G9a-null: *Tnnt2-rtTA;Tre-Cre;G9a*$^{f/f}$ mice. (O) Quantification of cardiac fibrosis in control and G9a-null mice lacking myocardial *G9a* 14 days after TAC operation. Ctrl: control mice. G9a-null: *Tnnt2-rtTA;Tre-Cre;G9a*$^{f/f}$ mice. (P) left ventricular internal dimension in diastole (LVIDd) and in systole (LVIDs) 14 days after TAC. Ctrl: control. G9a null: *Tnnt2-rtTA;Tre-Cre;G9a*$^{f/f}$ mice. P-value: Student's t-test. Error bar: SEM, standard error of the mean. (Q) Time course of left ventricular fractional shortening after TAC. (R) Ventricular weight/body weight ratio 8 weeks after TAC. (S) Left ventricular fractional shortening 8 weeks after TAC.

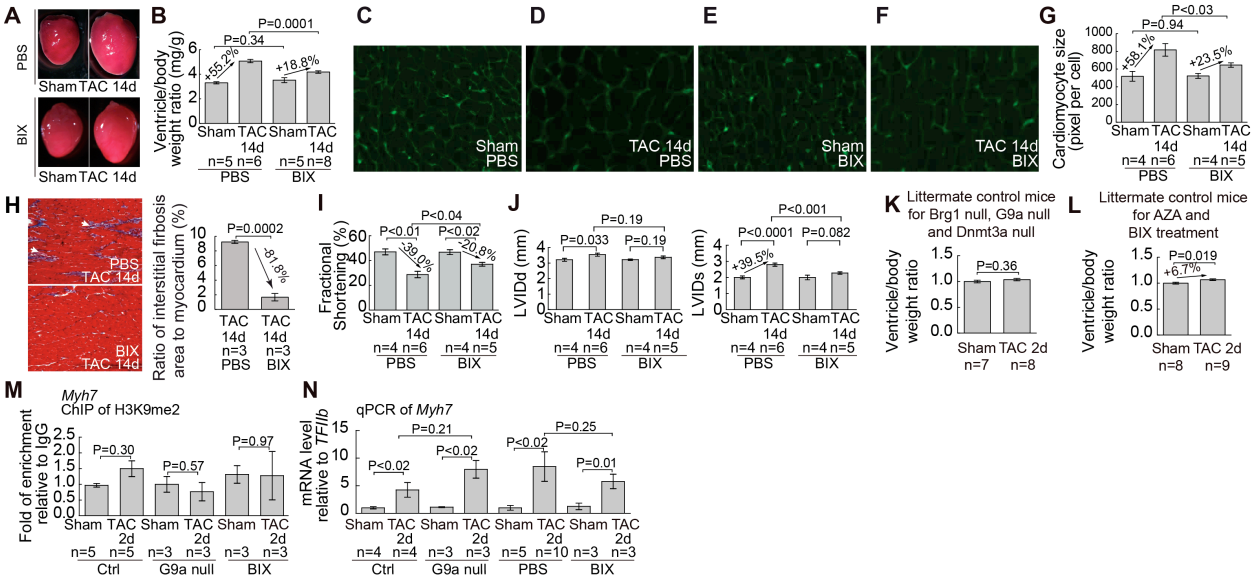

Supplemental Figure S3. H3K9 methylation by G9a/Glp underlies cardiac hypertrophy and dysfunction. (A and B) Gross morphology of ventricle (A) and quantitation of ventricle–body weight ratio (B) of PBS- and BIX-treated mice 14 days after the sham or TAC operation. PBS: phosphate buffered saline. P-value: Student's t-test. Error bar: SEM, standard error of the mean. (C–F) Wheat germ agglutinin (WGA) immunostaining of PBS- and BIX-treated mice 14 days after sham or TAC operation. (G) Quantitation of cardiomyocyte size of PBS- and BIX-treated mice 14 days after the sham or TAC operation. PBS: phosphate buffered saline. P-value: Student's t-test. Error bar: SEM, standard error of the mean. (H) Trichrome staining and quantification of cardiac fibrosis in PBS- and BIX-treated mice 14 days after TAC operation. Blue: fibrosis. (I and J) Echocardiographic measurement of fractional shortening (I), left ventricular internal dimension in diastole (LVIDd), and left ventricular internal dimension in systole (LVIDs) (J) of the left ventricle 14 days after TAC in PBS- and BIX-treated mice. P-value: Student's t-test. Error bar: SEM, standard error of the mean. (K and L) Ventricle/body weight ratio of mice 2 days after TAC. P-value: Student's t-test. Error bar: SEM, standard error of the mean. (M) Quantitation of H3K9me2 ChIP on the *Myh7* proximal promoter 2 days after sham or TAC operation. Ctrl: control heart. G9a null: *Tnnt2-rtTA;Tre-Cre;G9a*$^{f/f}$ heart. BIX: BIX-treated heart. P-value: Student's t-test. Error bar: SEM, standard error of the mean. (N) Quantitation of *Myh7* mRNA 2 days after sham or TAC operation. Ctrl: control heart. G9a null: *Tnnt2-rtTA;Tre-Cre;G9a*$^{f/f}$ heart. PBS: PBS-treated heart. BIX: BIX-treated heart. P-value: Student's t-test. Error bar: SEM, standard error of the mean.

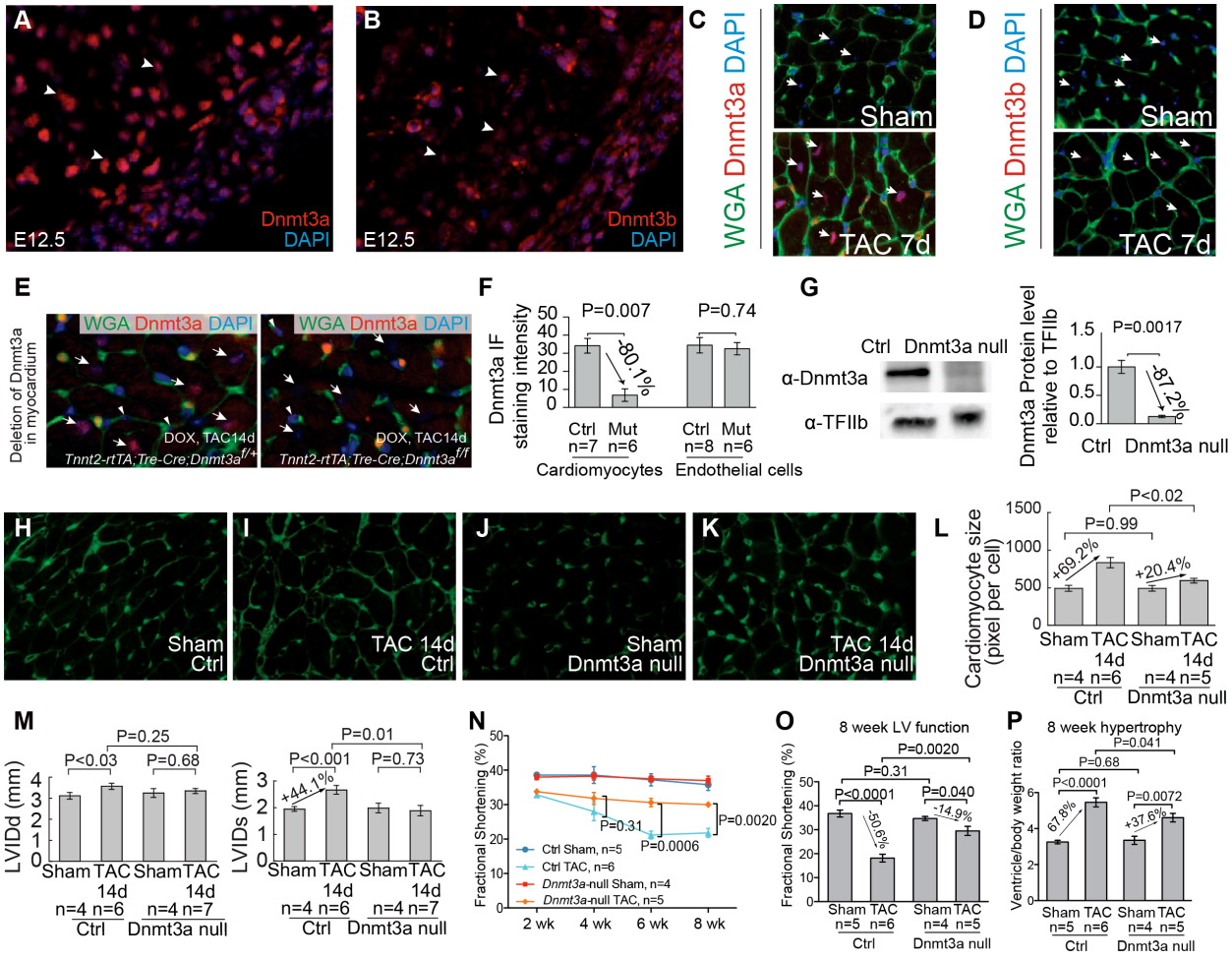

Supplemental Figure S4. Phenotype of the Dnmt3a conditional KO mice. (A and B) Immunostaining of Dnmt3a and Dnmt3b in the left ventricle of E12.5 embryos. Red: Dnmt3a or Dnmt3b. Blue: DAPI nuclear staining. Arrowheads point to nuclei of cardiomyocytes. (C and D) Immunostaining of Dnmt3a (C) and Dnmt3b (D) in adult hearts 7 days after sham or TAC procedure. Green: wheat germ agglutinin staining (WGA) outlining cell borders. Red: Dnmt3a or Dnmt3b immunostaining. Blue: DAPI nuclear staining. Arrows point to nuclei of cardiomyocytes. (E) Immunostaining of Dnmt3a in doxycycline (DOX)-treated littermate control (*Tnnt2-rtTA;Tre-Cre;Dnmt3a*$^{f/+}$) and Dnmt3a-null (*Tnnt2-rtTA;Tre-Cre;Dnmt3a*$^{f/f}$) hearts 14 days after TAC. The staining shows the absence of Dnmt3a proteins in cardiomyocytes (arrows) but not endothelial cells (arrowheads) in the heart of DOX-treated *Tnnt2-rtTA;Tre-Cre;G9a*$^{f/f}$ mice. Green: wheat germ agglutinin staining (WGA) outlining cell borders. Red: Dnmt3a immunostaining. Blue: DAPI nuclear staining. (F) Quantification of Dnmt3a immunofluorescence staining of control and Dnmt3a-null mice lacking myocardial *Dnmt3a* 14 days after TAC operation. Ctrl: control mice. Dnmt3a- null: *Tnnt2-rtTA;Tre-Cre;Dnmt3a*$^{f/f}$ mice. (G) Western blot and quantification of Dnmt3a in venticles of control and Dnmt3a-null mice lacking myocardial *Dnmt3a* 14 days after TAC operation. Ctrl: control mice. Dnmt3a-null: *Tnnt2-rtTA;Tre-Cre;Dnmt3a*$^{f/f}$ mice. (H–L) Wheat germ agglutinin (WGA) immunostaining of control (H and J) and Dnmt3a null mice lacking myocardial *Dnmt3a* (I and K), as well as quantitation of cardiomyocyte size (L) 14 days after sham or TAC operation. Ctrl: control mice. Dnmt3a null: *Tnnt2-rtTA;Tre-Cre;Dnmt3a*$^{f/f}$ mice. (M) Left ventricular internal dimension in diastole (LVIDd) and in systole (LVIDs) 14 days after TAC. Ctrl: control. Dnmt3a null: *Tnnt2-rtTA;Tre-Cre;Dnmt3a*$^{f/f}$ mice. P-value: Student's t-test. Error bar: SEM, standard error of the mean. (N) Time course of left ventricular fractional shortening after TAC. (O) Ventricular weight/body weight ratio 8 weeks after TAC. (P) Left ventricular fractional shortening 8 weeks after TAC.

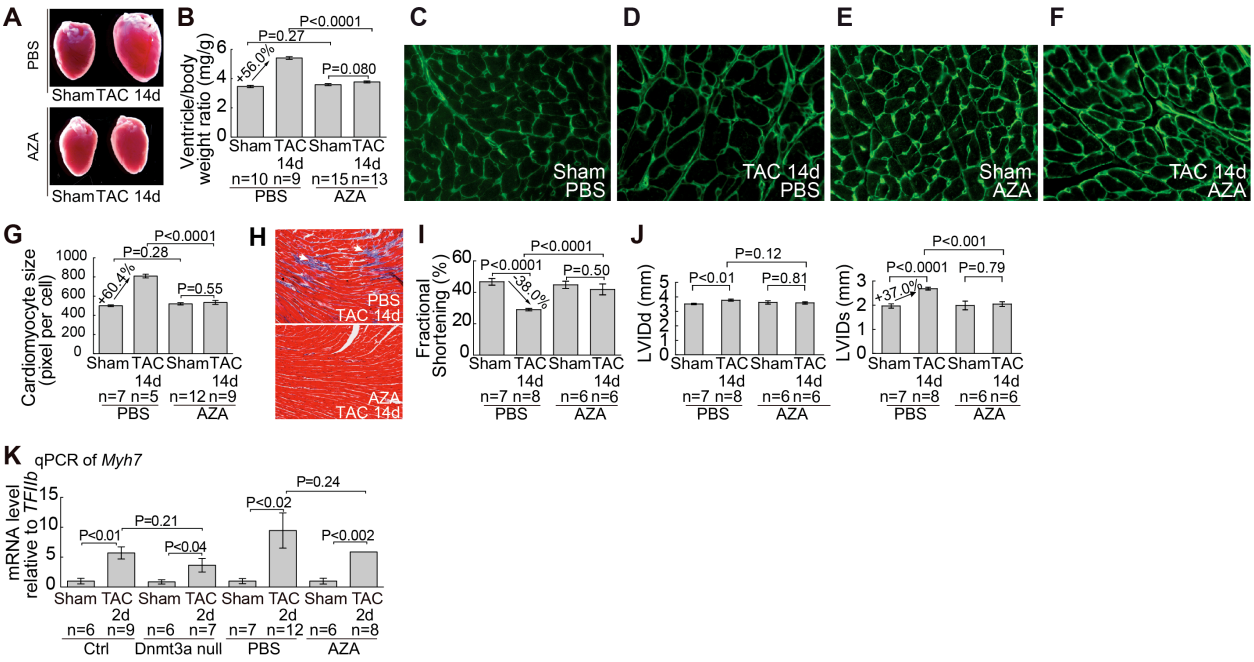

Supplemental Figure S5. DNA methylation by Dnmt3 is essential for cardiac hypertrophy and dysfunction. (A and B) Gross morphology of ventricle (A) and quantitation of ventricle–body weight ratio (B) of PBS- and AZA-treated mice 14 days after the sham or TAC operation. PBS: phosphate buffered saline. P-value: Student's t-test. Error bar: SEM, standard error of the mean. (C–F) Wheat germ agglutinin (WGA) immunostaining of PBS- and AZA-treated mice 14 days after sham or TAC operation. (G) Quantitation of cardiomyocyte size of PBS- and AZA-treated mice 14 days after the sham or TAC operation. PBS: phosphate buffered saline. P-value: Student's t-test. Error bar: SEM, standard error of the mean. (H) Trichrome staining of cardiac fibrosis PBS- and AZA-treated mice 14 days after TAC operation. Blue: fibrosis. (I and J) Echocardiographic measurement of fractional shortening (I), left ventricular internal dimension in diastole (LVIDd), and left ventricular internal dimension in systole (LVIDs) (J) of the left ventricle 14 days after TAC in PBS- and AZA-treated mice. P-value: Student's t-test. Error bar: SEM, standard error of the mean. (K) Quantitation of *Myh7* mRNA 2 days after sham or TAC operation. Data are presented as mRNA levels normalized to the sham-operated hearts in control mice or PBS-treated mice, respectively. Ctrl: control heart. Dnmt3a-null: *Tnnt2-rtTA;Tre-Cre;Dnmt3a*$^{f/f}$ heart. PBS: PBS-treated heart. AZA: AZA-treated heart. P-value: Student's t-test. Error bar: SEM, standard error of the mean.

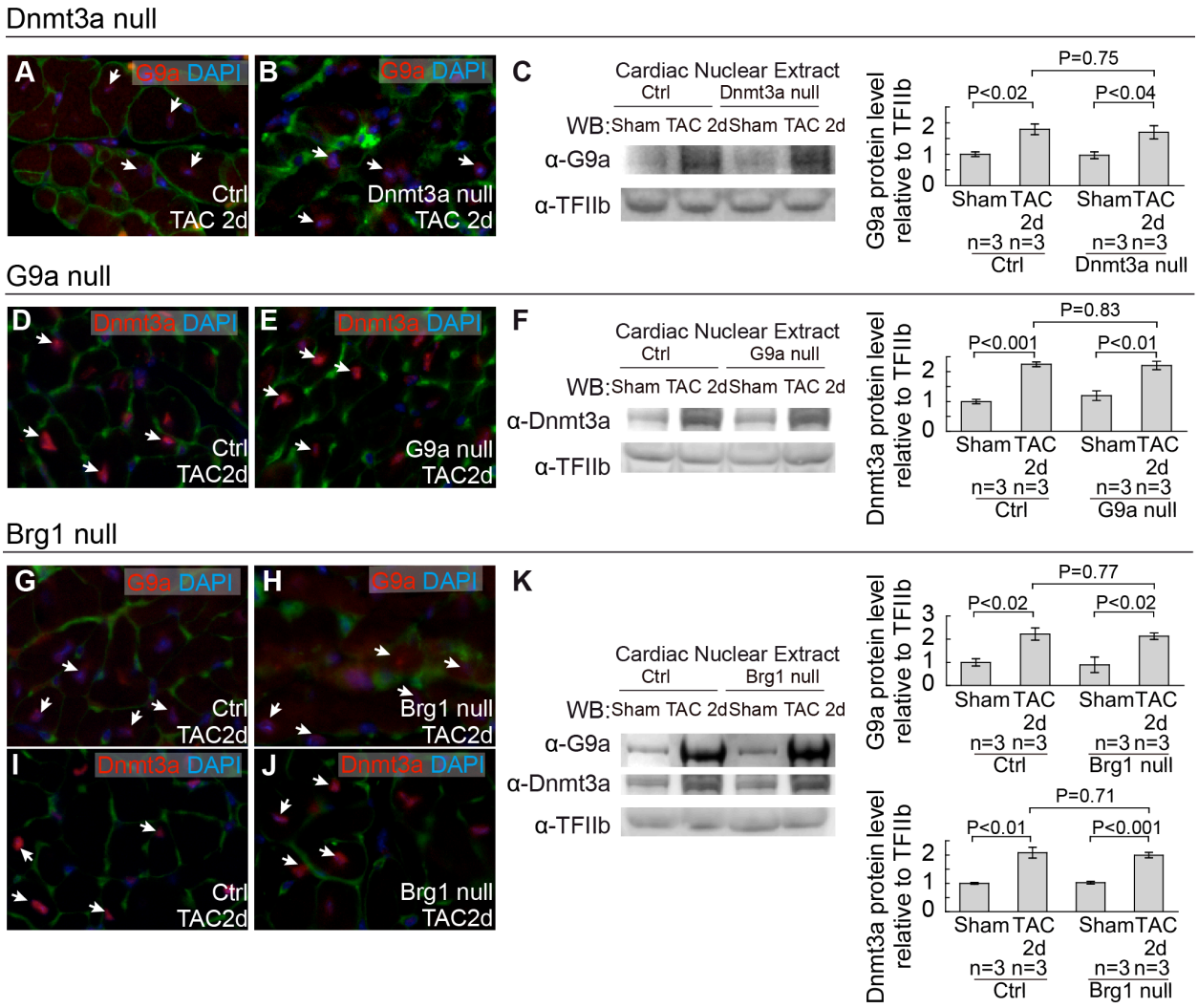

Supplemental Figure S6. Brg1, G9a, and Dnmt3a are not downstream targets of each other. (A and B) Immunostaining of G9a in control and Dnmt3a null (*Tnnt2-rtTA;Tre-Cre; Dnmt3a*$^{f/f}$) hearts 2 days after TAC. Green: wheat germ agglutinin staining (WGA) outlining cell borders. Red: G9a immunostaining. Blue: DAPI nuclear staining. Arrows point to nuclei of cardiomyocytes. (C) Western blot and quantitation of G9a proteins 2 days after TAC in control and Dnmt3a null hearts. TFIIb proteins were used as the internal control. P-value: Student's t-test. Error bar: SEM, standard error of the mean. (D and E) Immunostaining of Dnmt3a in control and G9a null (*Tnnt2-rtTA;Tre-Cre; G9a*$^{f/f}$) hearts 2 days after TAC. Green: wheat germ agglutinin staining (WGA) outlining cell borders. Red: Dnmt3a immunostaining. Blue: DAPI nuclear staining. Arrows point to nuclei of cardiomyocytes. (F) Western blot and quantitation of Dnmt3a proteins 2 days after TAC in control and G9a null hearts. TFIIb proteins were used as the internal control. P-value: Student's t-test. Error bar: SEM, standard error of the mean. (G–J) Immunostaining of G9a (G and H), Dnmt3a (I and J) in control and Brg1-null (*Tnnt2-rtTA;Tre-Cre;Brg1*$^{f/f}$) hearts 2 days after TAC. Green: wheat germ agglutinin staining (WGA) outlining cell borders. Red: G9a or Dnmt3a immunostaining. Blue: DAPI nuclear staining. Arrows point to nuclei of cardiomyocytes. (K) Western blot and quantitation of G9a, Dnmt3a proteins 2 days after TAC in control and Brg1 null hearts. TFIIb proteins were used as the internal control. P-value: Student's t-test. Error bar: SEM, standard error of the mean.

Control individuals with normal hearts

Age	Gender	Clinical features*	Cause of death	Anaylsis#
41	F	Normal LV wall thickness, EF=60%	Asphyxiation	D, q
32	F	Normal LV wall thickness, EF=50%, HTN	Anoxia	D, q
18	F	Normal LV wall thickness, EF=65%	Head trauma	D, q
50	M	Normal LV wall thickness, EF=55%	ICH	q, C
60	M	Normal LV wall thickness, EF>55%	Head trauma	q, C
47	M	Normal LV wall thickness, EF>55%	Head trauma	D, q

Patients with left ventricular hypertrophy

Age	Gender	Clinical features*	Cause of death	Anaylsis#
49	M	Mild LVH, EF=34%	ICH	D, q, C
46	M	Moderate LVH, EF=60%, HTN	Head trauma	D, q, C
28	F	LVH, EF=65%, morbid obesity	ICH	D, q, C
36	M	Moderate LVH, EF=72%, HTN	ICH	D, q
37	M	Mild LVH, EF=70%	Anoxia	D, q, C

*LV: left ventricle; EF: ejection fraction (normal > 50-55%); ICH: intracranial hemorrhage
LVH: left ventricular hypertrophy; HTN: hypertension

#Analysis performed based on the quality and amout of materials available for each assay.
D: DNA methylation assay; q: quantitive PCR; C: ChIP-qPCR assay

Supplemental Figure S7. Demography of heart transplantation donors. The left ventricular wall thickness and function was assessed by echocardiography or cardiac magnetic resonance imaging. Tissue assays performed include DNA methylation (D), RT–qPCR (q), and/or ChIP–qPCR (C). Not all assays could be performed in a given tissue sample due to the quality and amount of tissue materials available. LV: left ventricle. EF: ejection fraction (normal value is 55–65%). IHC: intracranial hemorrhage. BMI: body mass index (normal value is less than 25). LVH: left ventricular hypertrophy. HTN: hypertension.

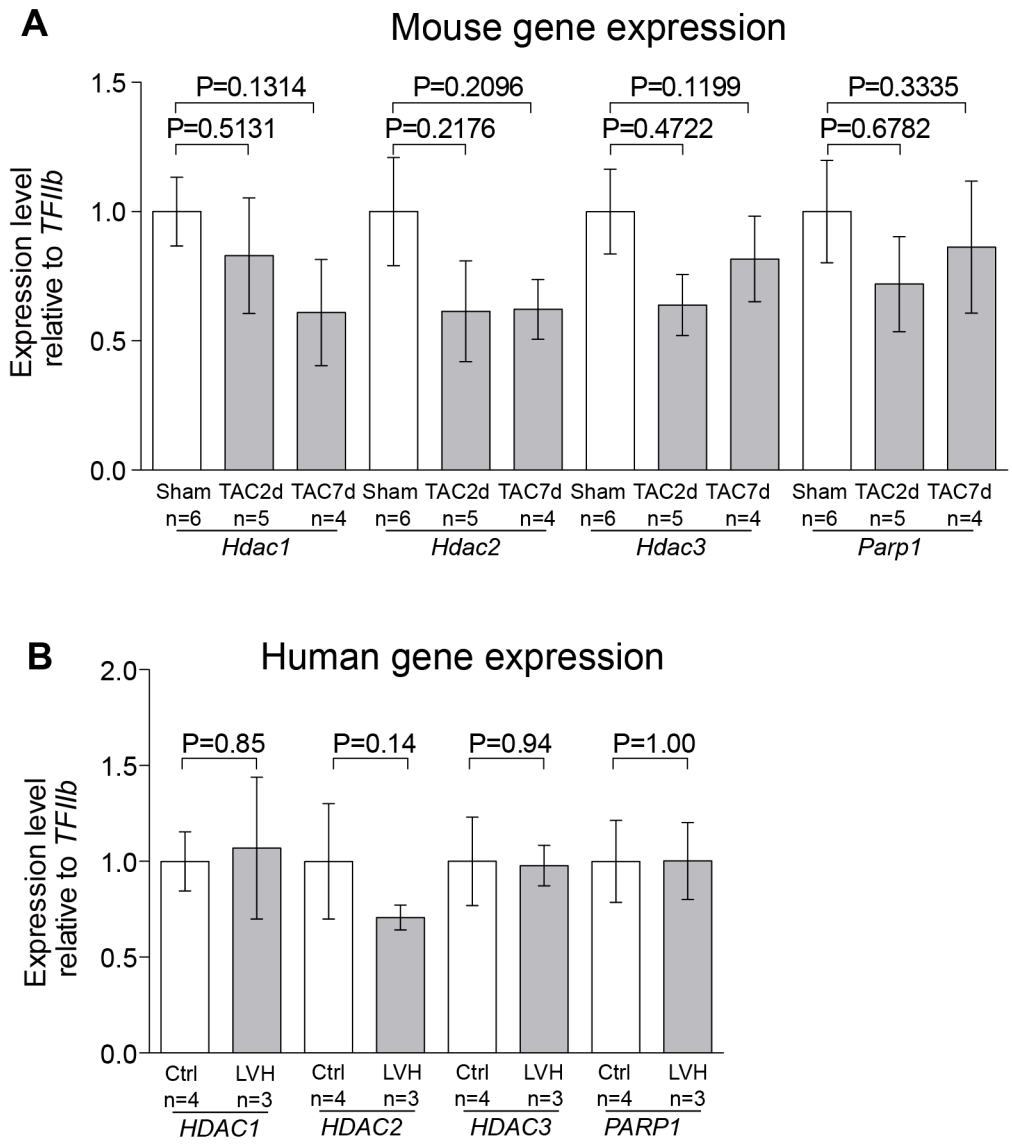

Supplemental Figure S8. Expression of HDAC 1, 2, 3 and PARP1 in mouse and human hypertrophic hearts. (A) mRNA expression of Class I Hdac genes (*Hdac1*, *2*, *3*) and *Parp1* in adult mouse hearts after sham, 2 or 7 days of TAC procedure. P-value: Student's t-test. Error bar: SEM, standard error of the mean. (B) mRNA expression of Class-I *HDAC* genes (*HDAC1*, *2*, *3*) and *PARP1* in normal and hypertrophic left ventricles of human hearts. Ctrl: control. LVH: left ventricular hypertrophy. P-value: Student's t-test. Error bar: SEM, standard error of the mean.